frontiers | Frontiers in Marine Science

TYPE Original Research
PUBLISHED 20 February 2023
DOI 10.3389/fmars.2023.1107530

OPEN ACCESS

EDITED BY
Tim Rixen,
Leibniz Centre for Tropical Marine Research (LG), Germany

REVIEWED BY
Peter Feldens,
Leibniz Institute for Baltic Sea Research (LG), Germany
Qiliang Sun,
China University of Geosciences Wuhan, China
Jian Hua Gao,
Nanjing University, China

*CORRESPONDENCE
Daidu Fan
ddfan@tongji.edu.cn

SPECIALTY SECTION
This article was submitted to Coastal Ocean Processes, a section of the journal Frontiers in Marine Science

RECEIVED 25 November 2022
ACCEPTED 02 February 2023
PUBLISHED 20 February 2023

CITATION
Song L, Fan D, Su J and Guo X (2023) Controls on shallow gas distribution, migration, and associated geohazards in the Yangtze subaqueous delta and the Hangzhou Bay.
Front. Mar. Sci. 10:1107530.
doi: 10.3389/fmars.2023.1107530

Controls on shallow gas distribution, migration, and associated geohazards in the Yangtze subaqueous delta and the Hangzhou Bay

Lei Song[1], Daidu Fan[1,2]*, Jianfeng Su[1,3] and Xingjie Guo[1,4]

[1]State Key Laboratory of Marine Geology, Tongji University, Shanghai, China, [2]Laboratory of Marine Geology, Qingdao National Laboratory for Marine Science and Technology, Qingdao, China, [3]Zhoushan Field Scientific Observation and Research Station for Marine Geo-hazards, China Geological Survey, Zhoushan, China, [4]Shanghai Institute of Geological Survey, Shanghai, China

Shallow gas is generally extensively distributed in the Holocene muddy sediments and gas seepage has been increasingly reported to induce geohazards in coastal seas, but controls on gas distribution and migration remain elusive. This study explores gas distribution and migration in the Yangtze subaqueous delta and the Hangzhou Bay using high-resolution acoustic profiles and core data. Shallow gas is widely detected by the common presence of acoustic anomalous reflections including enhanced reflection, gas chimney, bright spot, acoustic blanking, and acoustic turbidity. The gas front depth is generally less than 17.5 m, and is meanly shallower in the Hangzhou Bay than in the Yangtze subaqueous delta because of relatively shallower water depth and coarser Holocene sediments in the Hangzhou Bay. Shallow gas is inferred to be a biogenic product, and its distribution is highly contingent on the Holocene stratal thickness and water depth. Active gas migration and seepages are evident, and recently increasing occurrences of gas seepage can be ascribed to global warming and seabed erosion due to sediment deficit. The findings warn us to pay more attention to the positive feedback loops of gas seepages with global warming and seabed erosion for the associated geohazard prediction and reduction, typically in the highly developed coastal regions.

KEYWORDS

shallow gas, acoustic reflection, gas distribution, seabed instability, Yangtze Delta

1 Introduction

Shallow gas usually refers to the gas accumulated in the sub-bottom sediments within 1,000 m of depth (Fleischer et al., 2001). According to gas formation mechanisms, shallow gas can be divided into biogenic gas and thermogenic gas (Floodgate and Judd, 1992; Ye et al., 2003). Shallow gas is usually a biogenic product in shallow water sediments (Li et al., 2010), of which methane (CH_4) is the primary component (Hovland and Judd, 1988; Hu et al., 2012).

The gas can migrate upward from the host sediments to produce seepages, potentially forming pockmarks on the seafloor and gas plumes in the water column (Chen et al., 2017; Chen et al., 2020). If the gas escapes further from seawater into the atmosphere, it should accelerate global warming significantly because CH_4 is a greenhouse gas with 20–40 times higher radiative efficiency than CO_2 (Letcher, 2019; IPCC, 2021). In the past few decades, the content of CH_4 in the atmosphere has been increasing at a rate of approximately 0.5%–1% per year (Rasmussen and Khalil, 1986; IPCC, 2021). Annual global CH_4 emission from natural geological sources is estimated at 18–63 Mt, and marine gas leakage contributes 5–10 Mt annually (Etiope and Schwietzke, 2019; Etiope et al., 2019). Approximately 20% of total CH_4 emission to the atmosphere is inferred to be sourced from shallow coastal seas, consequently attracting increased research concerns (Fleischer et al., 2001; Jaśniewicz et al., 2019).

Seismic and acoustic explorations have been widely used for investigating gas-related anomalous reflections and mapping gas distribution in sub-bottom sediments (Ye et al., 2003; Hu et al., 2012; Cukur et al., 2013; Schneider von Deimling et al., 2013: Hu et al., 2016; Yang et al., 2019). Because gas-charged sediments can effectively absorb and scatter the energy of sound waves, which rapidly attenuate inner gas-charged sediments along the vertical direction (Hovland and Judd, 1988; Ye et al., 2003; Coughlan et al., 2021; Toker and Tur, 2021; Yang et al., 2022b), stratal structures usually display acoustic anomalous reflections including acoustic turbidity, acoustic blanking, enhanced reflection, bright spot, gas chimney, and pockmark (Ye et al., 2003; Visnovitz et al., 2015; Coughlan et al., 2021; Toker and Tur, 2021). Shallow gas has been surveyed to be widely distributed in coastal zones, such as the Gulf of Mexico, the Baltic Sea, and the East China Sea (Hovland and Judd, 1988; Zhang et al., 2004; Zhang et al., 2008; Lin et al., 2015; Liu et al., 2019; Chen et al., 2020). Abundant organic matter and suitable environmental conditions are conceivably vital for microbial growth to generate biogenic gas (Lin et al., 2015; Feng, 2017). Shallow biogenic gas generally appears when the Holocene sediments reach a certain thickness (García-García et al., 2007; Flury et al., 2016; Chen et al., 2020). However, most of the CH_4 produced in shallow sediments can be consumed by anaerobic oxidation of methane (AOM) when CH_4 diffuses upwards (Mogollón et al., 2012; Mogollón et al., 2013). It is generally believed that sulfate is the most important electron acceptor in AOM, and the zone where sulfate reduction and AOM occur most strongly is called the sulfate-methane transition zone (SMTZ) (Mogollón et al., 2013; Flury et al., 2016). CH_4 produced in organic-rich sediments below the sulfate reduction zone may cause the dissolved CH_4 to become oversaturated in pore water, consequently forming gas bubbles that accumulate to produce shallow gas in the sediments (Fleischer et al., 2001).

Shallow gas has been reported to be widely distributed in the post-LGM (last glacial maximum) strata in the Yangtze Delta and the Hangzhou Bay (Li et al., 2008; Hu et al., 2016; Xu et al., 2017; Wang et al., 2018). Thick muddy strata are indicated to be rich in organic matter and formed in an anoxic setting, favoring biogenic gas generation (Lin et al., 2015; Zhang and Lin, 2017). The top border of shallow gas is named the gas front, and its depth generally varies in a wide range from a few meters to tens of meters below the seafloor (Ye et al., 2003; Hu et al., 2016; Wang et al., 2018). Though a few studies have been carried out for acoustic identification and morphological characteristics classification of shallow gas in the Yangtze subaqueous delta and the Hangzhou Bay (Hu et al., 2016; Wang et al., 2018), quantitative analyses of gas distribution and front depth have been little reported. Chen et al. (2020) proposed that the thickness of the Holocene mud wedge is a key factor to determine the front depth of shallow gas, but its internal logic and other factors need additional exploration.

The gas-charged sediments have long been considered marine geologic hazards in terms of several aspects. The shear strength of sub-bottom sediments will be reduced obviously after filling with dissolved CH_4, and they are more susceptible to liquefaction under the influence of currents and waves (Sills and Wheeler, 1992; Wang and Liu, 2016; Song et al., 2021). Typically, sediment liquefaction likely occurs during extreme events such as typhoons, producing the collapse of marine constructions (Sumer et al., 2006; Wang et al., 2016; Wang and Liu, 2016; Wang et al., 2019; Wang et al., 2020). Meanwhile, sediment deficit due to dam constructions and other anthropogenic activities has caused severe erosion in the Yangtze subaqueous delta and the Hangzhou Bay (Xie et al., 2013; Guo et al., 2021), which has been accused to activate gas seepages because of thinning low permeability layer above gas-charged sediments (Chen et al., 2020). Considering the shallow burial depth of shallow gas in the study area, the effect of seabed erosion on gas preservation needs further investigation.

Therefore, this study is dedicated to identifying shallow gas-related anomalous acoustic reflections and mapping the gas front depth in the Yangtze subaqueous delta and the northern Hangzhou Bay, where the sedimentation regime has recently shifted from rapid deposition into severe erosion due to sediment deficit (Xie et al., 2013; Guo et al., 2021). Then, acoustic and core data are combined to probe the important influencing factors on gas distribution patterns. Ultimately, potential geological hazards related to recent shallow gas activities will be discussed.

2 Study area

The study area consists of the Yangtze subaqueous delta and the Hangzhou Bay (Figure 1). The Yangtze Estuary is influenced by semidiurnal tides, and the average tidal range is 2.6 m with a maximum tidal range of 4.6 m (Fan et al., 2004; Fan et al., 2017). The estuary is influenced more frequently by wind waves and less by swells. The Hangzhou Bay features a funnel shape with a rapid landward increase in tidal ranges (Ni et al., 2003; Xie et al., 2013; Xie et al., 2017). Due to the effect of the Coriolis force, the high tide level on the north shore is much higher than that on the south shore, while the low tide level on the south shore is higher than that on the north shore, resulting in a greater tidal difference between the opposite shores of the Hangzhou Bay (Yang et al., 2011; Luan et al., 2021). The bay is mainly influenced by wind waves, and large waves are induced by typhoons in summer and cold fronts in winter (Liu, 2019).

Deep incised valleys of a few tens of meters were formed at the present Yangtze Delta and the Hangzhou Bay during the LGM when the sea level dropped >130 m below the present sea level (Li et al., 2008; Li et al., 2014; Su et al., 2020). These paleo-incised valleys experienced rapid filling after the post-LGM transgression (Li et al.,

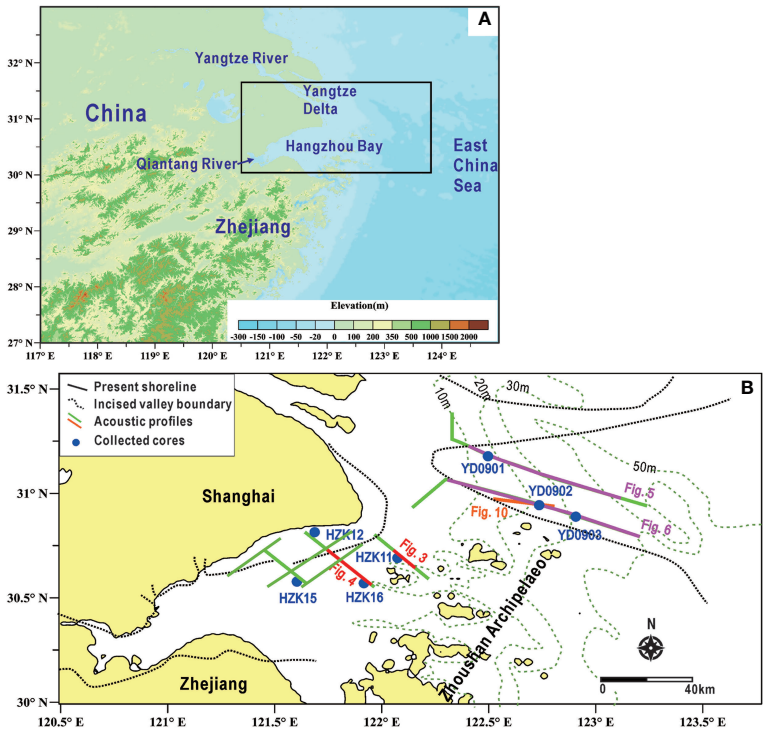

FIGURE 1
Geographical locations of the Yangtze Delta and the Hangzhou Bay **(A)**, and the distribution of shallow acoustic survey profiles and cores **(B)**. Light green dashed lines with numbers denote isobaths in meters.

2008; Zhang et al., 2013a; Lin et al., 2015; Zhang and Lin, 2017; Su et al., 2020). Transgressive surface (TS) is considered as the bottom interface during initial transgression, and maximum flooding surface (MFS) was formed during maximum transgression, occurring at 7.5 ka BP in the present Yangtze Delta area (Li et al., 2014; Su et al., 2017). The transgressive system tract (TST) represents deposition occurring between TS and MFS, and the highstand system tract (HST) is formed above MFS. The HST is further subdivided into early highstand system tract (E-HST) and late highstand system tract (L-HST) using the isochron of 2 kyr BP. Thick Holocene fine-grained sediments bear high TOC content of 0.54%–1.13% (Wang et al., 2012; Zhan et al., 2012), favoring shallow biogenic gas generation (Lin et al., 2010; Zhang et al., 2013a; Lin et al., 2015).

Annual average runoff of the Yangtze River at the Datong gauging station varied insignificantly in the past 60 years (Luan et al., 2021; Yang et al., 2022). However, the suspended sediment discharge has decreased dramatically by approximately 70% after the operation of the Three Gorges Dam (TGD) (Guo et al., 2021). Accordingly, the Yangtze subaqueous delta has shifted from rapid siltation to remarkable erosion, and erosion has recently expanded toward the Hangzhou Bay, which formerly receives a huge sediment supply from the Yangtze Estuary through strong tides (Xie et al., 2013; Xie et al., 2017).

3 Data and methods

Two acoustic surveys were carried out in July 2011 and August 2012, respectively. Acoustic profiles in the Yangtze subaqueous delta were collected in 2011 by the EdgeTech 3200XS Sub-Bottom Profiling System with the frequency 0.5–8 kHz at a ship speed of 4–5 kn (Figure 1B). It can penetrate 50 m or more below the seafloor, with a good vertical resolution of 0.12 m. In 2012, the GEO-SPARK2000 Electric Spark System was employed to collect acoustic profiles in the Hangzhou Bay with the frequency 8 kHz at a ship speed of 5 kn, fired at 400-ms intervals with the power of 2,000 J. Theoretically, it can detect the stratigraphic information range of 60 to 70 m below the seafloor. Towing observation operation and differential global positioning system were adopted in two surveys.

SonarWiz 5 software was applied to process all acoustic data (https://chesapeaketech.com/). After gain adjustment, automatic TVG compensation, and filtering technology, all profiles achieve the most effective visualization effect, typically reducing the banding phenomena due to discontinuities at the swath edges. After the interpretation of anomalous acoustic reflections, the gas front was identified and marked in each profile. To calculate the sediment thickness conveniently, the acoustic wave propagation velocity in sediments is set to 1,500 m/s (Chen et al., 2020). The distribution of shallow gas front depths was mapped using DIVA gridding interpolation in professional Ocean Data View software. DIVA, short for data-interpolating variational analysis, is a software tool dedicated to the spatial interpolation of *in situ* oceanographic data on a regular grid in an optimal way (https://www.seadatanet.org/Software/DIVA) (Beckers et al., 2014).

Stratal comparison in the study area was conducted using data from eight cores obtained from published papers (Table 1). Published ^{14}C ages were converted into calendar years BP using the Calib Rev. 8.2 program (http://calib.qub.ac.uk/calib/calib.html), and marine

biological samples were calibrated with the Marine20 curve and plant debris or organic-rich sediments with the IntCal20 curve (Stuiver and Reimer, 1993; Su et al., 2020). Meanwhile, the marine radiocarbon reservoir effect (ΔR) of −96 ± 60 yr was adopted here (Southon et al., 2002; Su et al., 2020). After that, the calibrated ^{14}C ages under 2σ confidence intervals were selected and took their median ages as the final calibrated ages (Table 2).

4 Results

4.1 Anomalous acoustic reflections of shallow gas in sediments

Acoustic reflection characteristics of gas-charged sediments are different from gas-free sediments. Gas-charged sediments can significantly absorb and scatter the energy of sound waves, making it difficult to reflect the information of stratal internal structures. Through interpretation and classification of anomalous acoustic reflections in the study area, the anomalies include bright spots, enhanced reflections, gas chimneys, acoustic blanking, acoustic turbidity, phase reversal, and pockmark (Figure 2). Among them, the first five anomalous acoustic reflections were used to identify the presence of shallow gas in the strata.

Bright spots are characterized by strong amplitude reflection at the gas front, featuring the polarity reversal of in-phase axes of normal seismic unit interfaces (Figure 2A). Generally, the extension of bright spots in the study area is less than 1 km, occurring within 10 m below the seafloor. If gas chimneys were found below bright spots, they should be caused by gas migration from the deeper sediments (Figure 2A).

Enhanced reflections show similar strong amplitude characteristics to bright spots, but their extension can be significantly longer than bright spots (Figure 2A). Enhanced reflections can extend more than 10 km in length, showing continuous irregular strong reflections (Figure 3). It is generally believed that enhanced reflections should occur at the topmost gas-charged organic-rich sediments in the sand (Judd and Hovland, 2007). Due to the buoyancy of gas, its upward migration and accumulation should produce the irregular shape of the gas front in the inconsistent sediment lithology and permeability. The depth of enhanced reflections varies greatly from 2 m to more than 10 m below the seafloor (Figures 2A, 3), but is mostly distributed within 10 m.

Formation of the gas chimney is generally thought to be associated with gas migration upwards (Hustoft et al., 2010; Cukur et al., 2013). The gas chimney is characterized as a narrow area of vertical disturbances, where the reflection phase is undular and distorted (main performance is acoustic turbidity) compared with the surrounding horizontal and vertical gas-free sediments (Ye et al., 2003; Cukur et al., 2013; Toker and Tur, 2021) (Figures 2, 4). They serve as gas migration pathways from deep gas-charged sediments upwards. When the gas migrated upwards to reach but not penetrate the seafloor, mound-shaped features could be formed on the seabed (Figures 5, 6). When the gas could penetrate the seabed and escape, the gas plume was observed in the water column (Figure 6). Gas seepages result in the formation of submarine pockmarks. When submarine pockmarks were observed, evidence of gas migration was found in their underlain sediments (Figure 2B).

Acoustic turbidity is characterized by amorphous low-amplitude chaotic reflection, and the phase axis is chaotic and difficult to track (Figures 2B, 5, 6). Acoustic turbidity is commonly observed below enhanced reflections, bright spots, or inside gas chimneys (Figures 2, 5, and 6). As long as the sediment contains 1% of gas content, acoustic turbidity may appear (Fannin, 1980). The extension varies greatly from tens of meters inside gas chimneys to several kilometers below irregularly enhanced reflections (Figures 2A, 3). Acoustic blanking shows phase axis reflection suddenly becoming weak or even disappearing (Figure 2A). For acoustic turbidity and acoustic blanking, the internal structure of the strata is difficult to distinguish. The extension length of acoustic blanking can reach up to tens of kilometers (Figures 5, 6).

Regular gas-related reflections with clear borders can be divided into curtain-shaped, columnar-shaped, and chimney-shaped reflections according to their morphological characteristics (Figure 4). Curtain-shaped reflection having nearly vertical sidewalls refers to the horizontal extension area with a certain width of >1 km, and the gas front is nearly parallel to the bedding with the burial depth of 5–10 m below the seafloor. Columnar-shaped reflection having similar gas front and sidewall structures with the curtain-shaped reflection refers to the gas-bearing disturbance area with a limited horizontal width of 0.5–1.0 km, and the gas front depth is generally not more than 5 m. Compared with curtain-shaped and columnar-shaped reflections, chimney-shaped reflection is characterized by a smaller horizontal extension of <0.5 km and much shallower gas front, which can indicate the stronger upward migration and accumulation of gas.

TABLE 1 Summary information of cores used in this study (see Figure 1B for core locations).

Core	Water depth (m)	Length (m)	Lon. (E)	Lat. (N)	Source
HZK11	−10.8	60.8	122°04.586’	30°41.942’	Wang et al., 2018
HZK12	−10.8	96.9	121°41.300’	30°46.198’	Wang et al., 2018
HZK15	−13.0	53.6	121°36.327’	30°35.079’	Wang et al., 2018
HZK16	−10.0	123.0	121°55.132’	30°34.706’	Wang et al., 2018
YD0901	−21.0	65.2	122°30.011’	31°11.029’	Su et al., 2017
YD0902	−23.0	69.1	122°44.348’	30°56.999’	Su et al., 2020
YD0903	−36.0	60.2	122°54.550’	30°53.905’	Su et al., 2017

TABLE 2 ^{14}C age data selected from seven cores in the Yangtze subaqueous delta and the Hangzhou Bay (see Figure 1B for core locations).

Core ID	Depth (m)	Dating material	^{14}C age (yr BP)	Calibrated age (cal yr BP)			Source
				2σ range	Prob.	Median	
HZK11	2.22	Bivalve shell	950 ± 30	313–634	1	474	Wang et al., 2018
	6.5	Gastropod shell	1,510 ± 30	793–1,185	1	989	
	9.6	Gastropod shell	2,260 ± 30	1,588–2,016	1	1,802	
	11.1	Plant material	8,030 ± 40	8,750–9,020	0.98	8,885	
	13.03	Plant material	8,170 ± 30	9,010–9,149	0.71	9,080	
	14.58	Plant material	8,290 ± 40	9,191–9,427	0.84	9,309	
	20.5	Plant material	8,620 ± 40	9,532–9,682	1	9,607	
HZK15	11.2	Bivalve shell	7,800 ± 40	7,988–8,369	1	8,179	Wang et al., 2018
	11.5	Bivalve shell	6,520 ± 40	6,690–7,142	1	6,916	
	26.7	Bivalve shell	8,580 ± 40	8,940–9,394	1	9,167	
	29.15	Bivalve shell	9,330 ± 40	9,806–10,313	1	10,060	
	32.8	Bivalve shell	9,250 ± 40	9,709–10,206	1	9,957	
HZK16	9.5	Bivalve shell	7,640 ± 30	7,824–8,206	1	8,015	Wang et al., 2018
	23.76	Bivalve shell	9,140 ± 50	9,550–10,103	1	9,827	
	27.5	Bivalve shell	9,550 ± 50	10,156–10,628	1	10,392	
	27.82	Bivalve shell	9,640 ± 50	10,227–10,740	1	10,484	
	29.9	Bivalve shell	9,800 ± 40	10,487–11,049	1	10,768	
YD0901	1.57	Mollusk shell	765 ± 30	131–492	1	312	Su et al., 2017
	4.01	Mollusk shell	790 ± 30	151–502	1	327	
	7.13	Mollusk shell	1,435 ± 30	725–1,109	1	917	
	7.7	Mollusk shell	1,690 ± 30	986–1,345	1	1,166	
	13.5	Mollusk shell	3,085 ± 35	2,631–3,054	1	2,843	
	14.8	Mollusk shell	3,670 ± 35	3,327–3,765	1	3,546	
	20.78	Mollusk shell	5,470 ± 40	5,558–5,958	1	5,758	
	32.77	Mollusk shell	6,310 ± 40	6,438–6,887	1	6,663	
	33.21	Mollusk shell	6,350 ± 40	6,484–6,935	1	6,710	
YD0902	8.17	Snail	764 ± 36	659–731	1	695	Ren et al., 2019
	11.13	Shell	1,543 ± 37	842–1,238	1	1,040	Su et al., 2020
	14.07	Shell debris	2,416 ± 39	1,773–2,251	1	2,012	
	19.51	Sediments	4,703 ± 44	5,320–5,427	0.56	5,374	
	23.21	Sediments	8,791 ± 56	9,592–9,963	0.83	9,778	
	40.83	Sediments	10,325 ± 61	11,930–12,474	0.98	12,202	
YD0903	4.45	Mollusk shell	2,490 ± 30	1,882–2,309	1	2,096	Su et al., 2017
	9.59	Mollusk shell	3,200 ± 35	1,748–3,175	1	2,462	
	18.55	Mollusk shell	6,020 ± 40	6,153–6,570	1	6,362	
	22.04	Mollusk shell	7,400 ± 40	7,587–7,952	1	7,770	
	34.93	Mollusk shell	11,350 ± 60	12,601–13,007	1	12,804	
	47.58	Mollusk shell	13,090 ± 83	14,603–15,363	1	14,983	

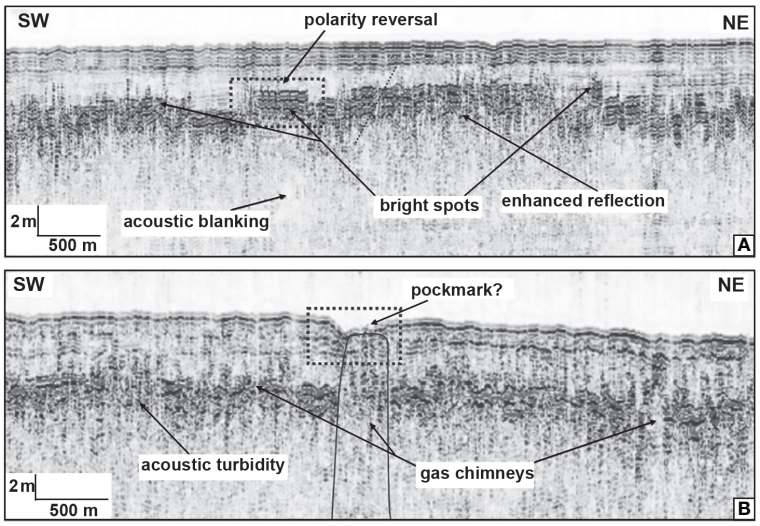

FIGURE 2
Identification and interpretation of main anomalous acoustic reflections in acoustic profiles, such as bright spot, enhanced reflection, polarity reversal, and acoustic blanking **(A)**; gas chimney, pockmark, and acoustic turbidity **(B)**.

4.2 Distribution and migration of shallow gas in sediments

The burial depth of the shallow gas front in the study area was mapped according to new sub-bottom acoustic data in this study and those by Chen et al. (2022). Shallow gas is widely distributed in the study area with the gas front depth ranging from 0 to 17.5 m. In comparison, gas front depths varying from 5 to 15 m in the Yangtze subaqueous delta are relatively deeper than those from 2 to 7.5 m in the Hangzhou Bay (Figure 7).

According to acoustic profiles collected in the Yangtze subaqueous delta in 2011 (Figures 5, 6), wide acoustic blanking zones were commonly found below the seafloor. Acoustic turbidity and acoustic basement could be seen between the two acoustic blanking zones (Figure 6). Seaward termination of acoustic blanking zones is present where the Holocene sediment thickness is 14 m (Figure 5) and 23.7 m (Figure 6), respectively. Because the high-altitude paleo-topography interrupts continuous variation of the Holocene sediment thickness, the distribution of acoustic blanking zones is disconnected until the Holocene sediment thickness reaches ~20.7 m (Figure 6). In the southern Yangtze subaqueous delta, gas front depths of two acoustic profiles show their different landward-changing patterns (Figures 5, 6). The gas front depth increases gradually landward along the acoustic profile across core YD0901 (Figure 5), while it increases landward first but ends with a landward decreasing trend along the acoustic profile across cores YD0902 and YD0903 (Figure 6).

In the northern Hangzhou Bay, a series of intermittent narrow acoustic blanking zones and acoustic turbidity zones were found (Figure 4). A few acoustic turbidity zones indicate that gas can migrate upwards from the deeper sediments (Figure 4). In this area, different characteristics of narrow acoustic blanking zones are associated with the gas distribution difference. If the locations of acoustic blanking zones or gas fronts were closely connected to enhanced reflections, they should have a high concentration of shallow gas with a remarkable tendency of upward migration (Figures 3, 4). However, some stratal internal structures can be diagnosed in the weak acoustic blanking zones that are not spatially interwoven with enhanced reflections, thus hinting at a relatively low concentration of shallow gas (Figure 4).

Gas plumes were observed in the water column, and some mounds were found on the seafloor in the Yangtze subaqueous delta (Figures 5, 6). The gas plumes rose ~5 m above the seafloor, and below the seafloor, gas chimney and acoustic turbidity could be

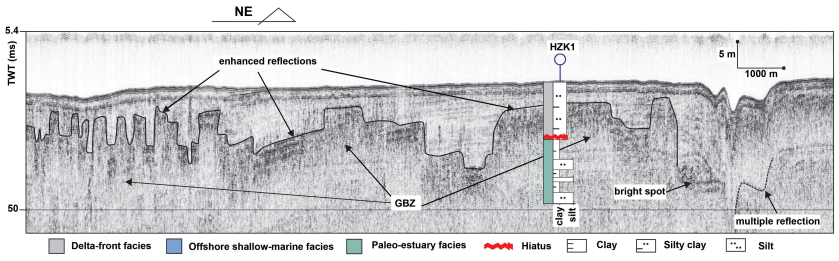

FIGURE 3
A shallow acoustic profile across core HZK11 to show irregular enhanced reflections by the presence of gas in shallow sediments in the Hangzhou Bay. GBZ is short for the gas-bearing zone. See Figure 1B for the locations of the profile and the core.

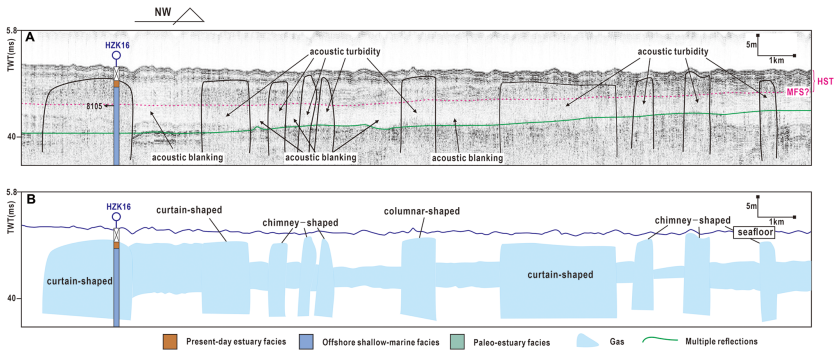

FIGURE 4
A shallow acoustic profile across core HZK16 to show different shapes of abnormal acoustic reflections by the presence of gas in shallow sediments in the Hangzhou Bay **(A)**, and interpretation of the presence of shallow gas in the acoustic profile **(B)**. See Figure 1B for the locations of the profile and the core.

identified (Figure 5). The mounds were approximately 1–2 m high, and their formation was also closely related to gas migration (Figures 5, 6). Pockmarks, with a maximum diameter of ~500 m, were observed in the Jinshan Deep Trough and near Yehuangpan island and Xiaojishan island in the northern Hangzhou Bay, and gas-related acoustic blanking and acoustic turbidity were well developed below the pockmarks. Meanwhile, pockmarks generally are accompanied by enhanced reflections and gas chimneys (Figure 8). The pockmarks with diameters exceeding 20 m were also found in the Yangtze subaqueous delta (Figure 8).

5 Discussion

5.1 Possible source for shallow gas

Shallow gas can be generated by biogenic (generally $\delta^{13}C_{CH4}$ ~ −110‰−60‰, δD_{CH4} <110‰) or thermogenic processes (generally $\delta^{13}C_{CH4}$ >60‰, δD_{CH4} >110‰) (Whiticar, 1999; Ye et al., 2003; Feng, 2017). The low $\delta^{13}C$ values and heavy hydrocarbon contents of shallow gas in core sediments retrieved from the Yangtze delta plain (Zhang et al., 2013a; Feng, 2017) and the southern coastal plain of Hangzhou Bay (Yang et al., 2021) indicate its biogenic origin.

In the Yangtze subaqueous delta and the Hangzhou Bay, shallow gas can be detected extensively as shown by acoustic blanking and acoustic turbidity (Figures 4–6). The gas front is distributed in the Holocene sediments of HST and TST, and its burial depth is mostly shallower than 17.5 m (Figure 7). Meanwhile, anomalous acoustic reflections were not observed in the thin Holocene sediments. Thus, the shallow gas is presumed to be biogenic gas within the Holocene deltaic or estuarine sediments.

The generation of shallow biogenic gas requires abundant organic matter in sediments to be used by methanogenic bacteria (Lin et al., 2015; Feng, 2017). The content of total organic carbon (TOC) in cores CJK08, YD0901 (Wang et al., 2012), and ZK9 (Zhan et al., 2012) is generally >0.5%, high enough for the occurrence of microbial

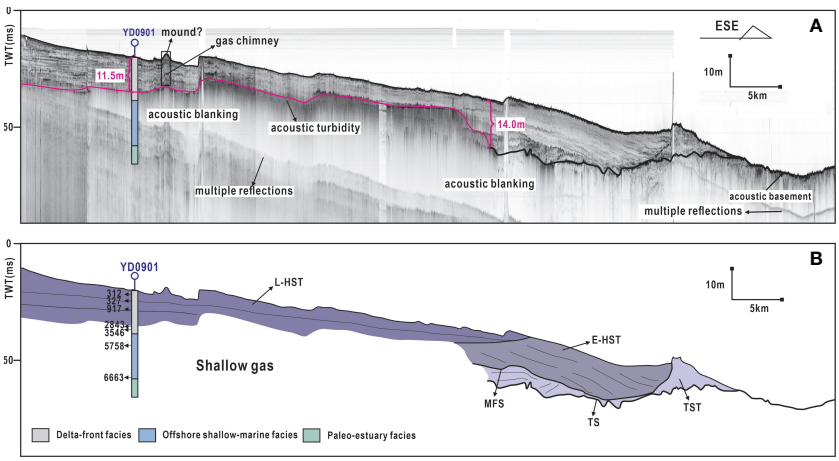

FIGURE 5
A shallow acoustic profile across core YD0901 to show gas-related anomalous reflections in the Yangtze subaqueous delta **(A)**, and interpretation of the profile **(B)**. See Figure 1B for the locations of the profile and the core. The purple line marks the gas front. TS, Transgressive surface; TST, Transgressive system tract; MFS, Maximum flooding surface; E-HST, Early highstand system tract; L-HST, Late highstand system tract.

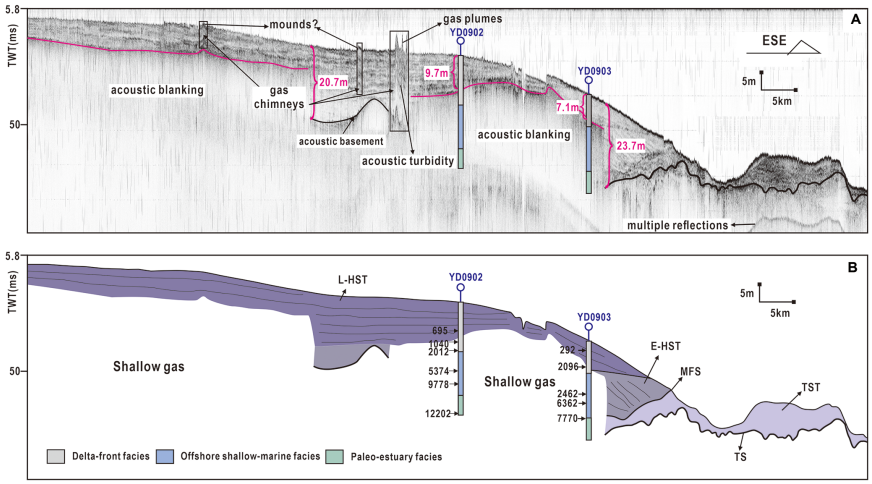

FIGURE 6
A shallow acoustic profile across cores YD0902 and YD0903 to show gas-related anomalous reflections in the Yangtze subaqueous delta **(A)**, and interpretation of the profile **(B)**. See Figure 1B for the locations of the profile and the cores. The purple line marks the gas front. TS, Transgressive surface; TST, Transgressive system tract; MFS, Maximum flooding surface; E-HST, Early highstand system tract; L-HST, Late highstand system tract.

methanogenesis (Rice and Claypool, 1981). In comparison, the upper Holocene sediments in the Yangtze subaqueous delta usually have much higher TOC content (TOC ~ 0.54%–1.13%, Wang et al., 2012; Zhan et al., 2012) than those in the Yangtze delta plain (Zhang et al., 2013b). However, shallow gas is little found in the former strata because therein CH_4 production could be mostly consumed by sulfate reduction in marine sediments (Mogollón et al., 2012; Mogollón et al., 2013; Flury et al., 2016). The gas front has often been detected to locate near the bottom boundary of the delta-front facies (Figures 5, 6), indicating that shallow gas should be sourced from the deeper Holocene sediments by upward migration and accumulation in the Yangtze subaqueous delta and the Hangzhou Bay.

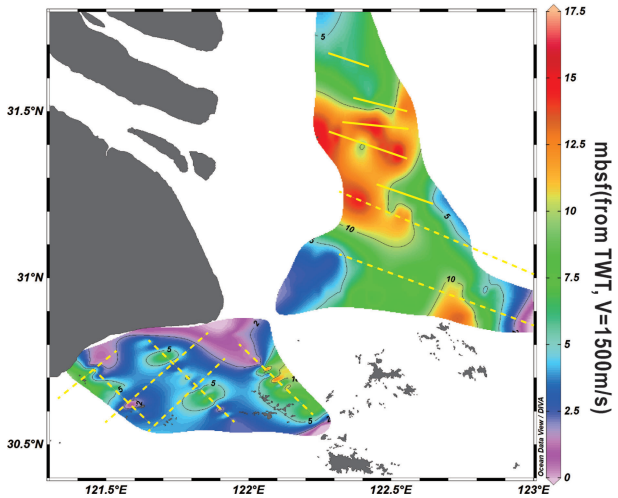

FIGURE 7
The contour map of burial depths of the shallow gas front in the Yangtze subaqueous delta and the Hangzhou Bay. The data of gas front depths in the northern Yangtze subaqueous delta are retrieved from Chen et al. (2022). Dashed yellow lines indicate the acoustic profiles acquired in this study, and solid yellow lines show the acoustic profiles investigated by Chen et al. (2022). Dashed black lines represent the isobaths.

5.2 Controlling factors of gas distribution

Shallow gas was usually found in relatively thicker Holocene strata as shown by large-scale distributions of acoustic blanking and acoustic turbidity (Figures 5, 6). It might disappear as the Holocene strata suddenly taper out (Figure 6). Previous studies also concluded that the Holocene stratal thickness plays a key role in controlling shallow gas generation and accumulation (García-García et al., 2007; Flury et al., 2016; Chen et al., 2020). Part of the reason is that thicker fine-grained Holocene sediments with a higher abundance of organic matter tend to generate more CH_4, consequently increasing the upward CH_4 flux to shift the SMTZ towards the shallow depth (Flury et al., 2016). Moreover, enhanced methanogenesis should produce CH_4 supersaturation in sediments to generate CH_4 gas bubbles (García-García et al., 2007; Flury et al., 2016), causing its underlying gas-charged strata to not show clear internal stratal structures because of acoustic anomalous reflections.

Increasing water depth may increase the solubility of CH_4 in interstitial water, making it more difficult for biogenic CH_4 to form gas bubbles in shallow sediments (Ulyanova et al., 2012). This is shown by the acoustic profile across cores YD0902 and YD0903 where shallow gas could be detected in the Holocene strata with its thickness exceeding 20.7 m at the water depth of ~10 m, but the stratal thickness should exceed 23.7 m at the water depth of ~20 m (Figure 6). However, at the water depth of ~20 m along the acoustic profile across core YD0901, shallow gas was observed when the Holocene stratal thickness just exceeded 14.0 m (Figure 5). It is therefore suggested that water depth is an influencing factor but not a single determining factor on the shallow gas distribution in shallow sediments.

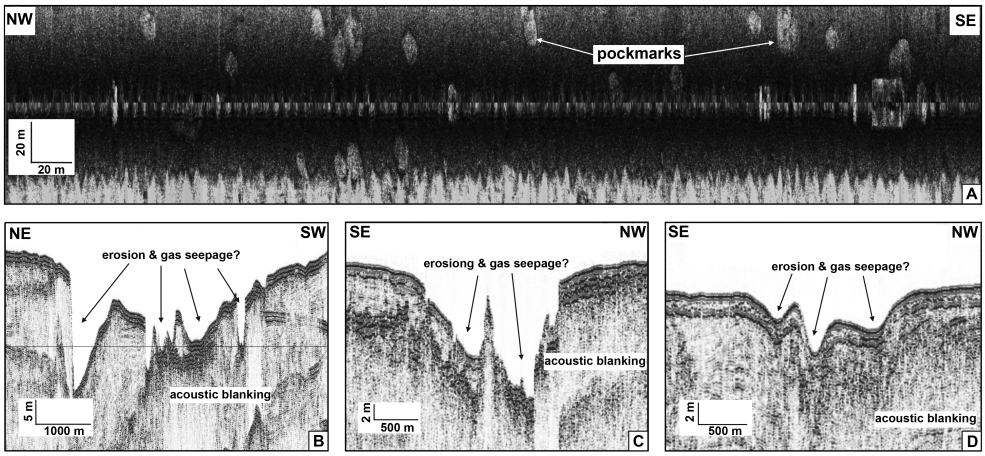

FIGURE 8
Gas-seepage-related structures in the Yangtze subaqueous delta and the Hangzhou Bay: **(A)** pockmarks detected by side-scan sonar (modified from Chen et al., 2022), and **(B–D)** seabed depressions induced by gas seepage activities disclosed by acoustic profiles.

Once the gas is generated, it tends to move upward due to buoyancy. However, upward gas migration requires overcoming the capillary force and the overburden pressure of overlying strata and water mass. Typically, the higher capillary force indicates the lower permeability of the sediment (Lin et al., 2010; Qu et al., 2013; Zhang et al., 2013b). In general, coarse-grained sediments are more beneficial for the gas surpassing capillary forces to migrate upward. The overburden pressure reduces as the water depth and/or the overlying strata thickness decrease. In the Yangtze subaqueous delta, the gas front was usually observed to locate in the delta-front facies (Figures 5, 6), and its burial depth might decrease towards the shallower water zone or the thinner stratal thickness of silt-dominated delta-front facies (Figures 6, 7, 9).

Compared with the Yangtze subaqueous delta, the gas front in the Hangzhou Bay was much shallower as a whole (Figure 7). Firstly, the mean water depth in the Hangzhou Bay is shallower than that in the Yangtze subaqueous delta, potentially leading to lower CH_4 solubility for the easier formation of CH_4 gas bubbles in the

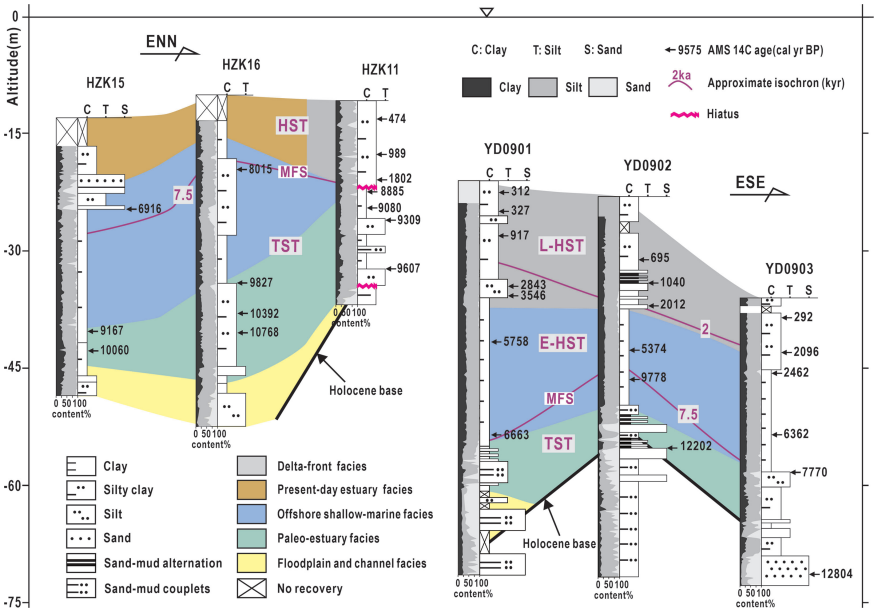

FIGURE 9
Core correlation profiles in the northern Hangzhou Bay and the Yangtze subaqueous delta show detailed information on lithology, sedimentary facies, chronology, and system tracts. The Holocene stratal base at ca. 11.7 ka BP was deduced from ^{14}C ages data of cores HZK11, HZK15, and HZK16 (Wang et al., 2018), and cores YD0901, YD0902, and YD0903 (Su et al., 2017; Ren et al., 2019; Su et al., 2020). See Figure 1B for the locations of the cores. TST, Transgressive system tract; MFS, Maximum flooding surface; E-HST, Early highstand system tract; L-HST, Late highstand system tract.

shallower sediments. Then, well-sorted estuarine sediment by intense tidal currents in the northern Hangzhou Bay should increase sediment permeability to ease gas upward migration (Figure 9). Moreover, recently increasing seabed erosion has been extensively observed in the northern Hangzhou Bay due to a sharp decrease in sediment input from the Yangtze River after the TGD construction (Xie et al., 2013; Xie et al., 2017; Guo et al., 2021). The seabed erosion rate in the northern Hangzhou Bay was about −0.4 m/yr during 2010–2014 (Xie et al., 2017), and the total scouring thickness at the Jinshan Deep Trough exceeded 2.4 m during the recent 30 years from 1989 to 2018 (Zhang et al., 2021). The seabed erosion has greatly reduced the thickness of cap sediments above the shallow gas, consequently lessening the overburden pressure of the gas to activate gas seepages in the Hangzhou Bay (Chen et al., 2020).

Gas front depth becoming shallower due to seabed erosion can also be observed in the Yangtze subaqueous delta (Figures 6, 10). According to the acoustic surveys, the gas front depth near YD0902 changed slightly from 9.7 m in July 2011 to 9.4 m in November 2017, which may be related to temperature changes (Martinez-Carreño and Garcia-Gil, 2013). According to the acoustic profiles, the average water depth on the west side was approximately 8.8 m in July 2011, and became 11.6 m in November 2017, indicating a seabed erosion thickness of approximately 2.8 m. Meanwhile, shallow gas front depth became shallow up to 3 m or even more at the inner Yangtze subaqueous delta (Figures 6, 10). A mound was found with its landward occurrence of a shallow acoustic turbidity zone in the seismic profile of 2017, both indicating upward gas migration activities (Figure 10). Meanwhile, the occurrence of huge negative topography at the inner delta front zone in 2017 was considered to be related with recently increasing seabed erosion in the Yangtze subaqueous delta with a water depth of 5–20 m because of sediment deficit (Yang et al., 2011; Chen et al., 2020; Guo et al., 2021).

In summary, gas distribution and accumulation in shallow deltaic/estuarine sediments are primarily determined by the stratal thickness and permeability of the Holocene sediments and water depth (Mogollón et al., 2012; Mogollón et al., 2013; Flury et al., 2016; Chen et al., 2020). Thicker Holocene strata and shallower water depth are favorable for gas generation and accumulation. Overburden pressure and low permeability of sediments above the shallow gas have significant effects on gas migration. Recently, gas migration is highly enhanced by increasing seabed erosion at the inner Yangtze delta front and the northern Hangzhou Bay due to sediment deficit, potentially triggering gas seepage and seabed instability events. Thus, more attention should be paid to this new situation for potential geological hazardous occurrences.

5.3 Implications of shallow gas-associated geological hazards

5.3.1 Gas seepage

Distinct gas seepage phenomena, such as gas plumes and pockmarks, have been commonly observed in the study area (Figures 5, 6, 8, 10). Gas seepage is closely related to gas migration in sediments. Below the gas plumes and pockmarks, gas chimneys should be visibly observed. The occurrences of mounds on the seabed and gas chimneys below the seafloor show their clear spatial overlap. The mounds are where the gas is trapped below the seabed sediments, conceivably being the initial form of pockmarks (Hovland and Judd, 1988; Koch et al., 2015; Nyman et al., 2020). When the gas pressure exceeds the overburden pressure in shallow sediments because of excessive gas accumulation or seabed erosion, it will cause the seabed sediments to dome upward. Once the accumulation pressure of the gas is high enough within the mounds, the gas will burst into the water column and the companion sediments will be carried away. Afterward, the positive topography of the mound structure should be replaced by the negative topography of pockmark structures (Chen et al., 2017).

The behavior and location of SMTZ are closely linked to the methanogenic efficiency and the gas front depth in shallow sediments. Data of Flury et al. (2016) clearly showed the changes of gas front depths and the SMTZ in gas-charged sediments and gas-free sediments, and the shallowing SMTZ promoted gas generation and accumulation in shallower sediments (Figure 11). Mogollón et al. (2013) also proposed that the gas front depth should take a key role in controlling CH_4 and sulfate diffusion fluxes toward the SMTZ. The shallower the gas front depth becomes, the greater the diffusion flux of CH_4 is. The latter has the potential to shift the SMTZ upward. In other words, the depth

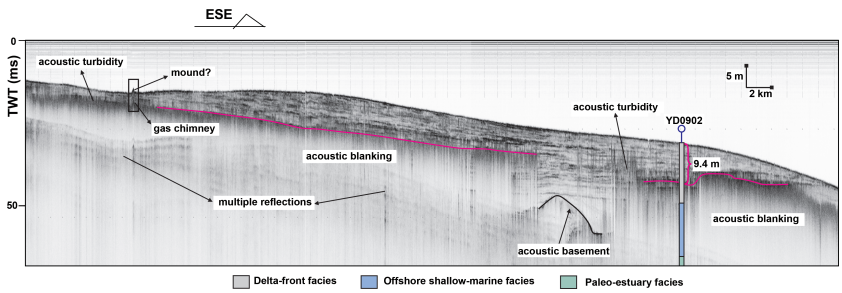

FIGURE 10
A shallow acoustic profile showing gas-related anomalous reflections in the Yangtze subaqueous delta. The purple line marks the gas front. The original acoustic profile was reproduced from Chen et al. (2022).

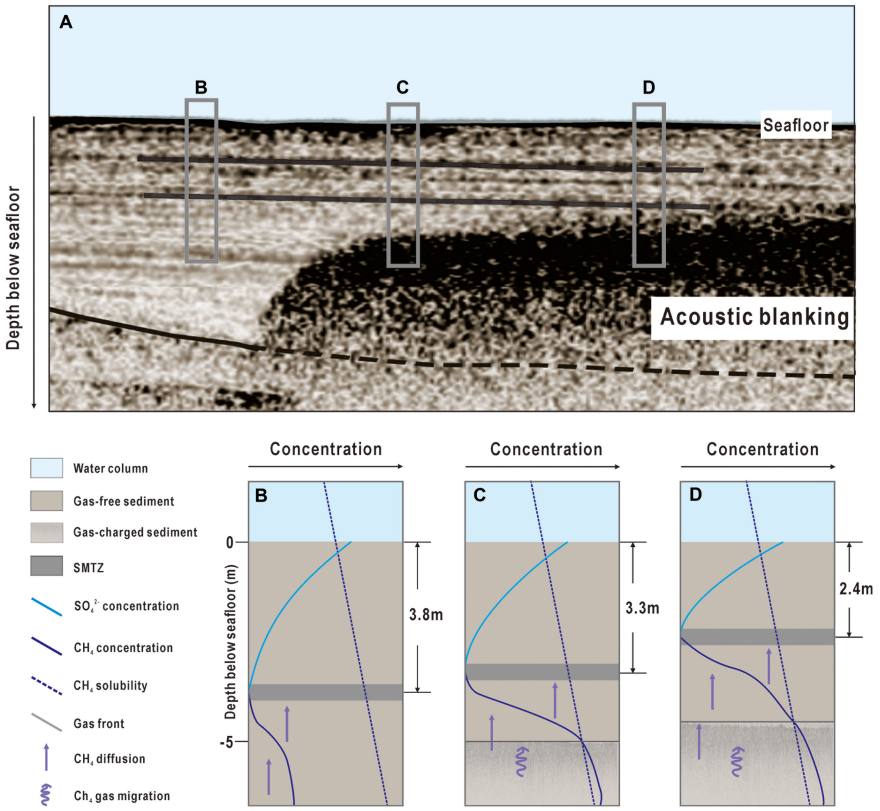

FIGURE 11
The chirp acoustic profile of gas-charged and gas-free sediment intersection area in the Aarhus Bay **(A)**, sulfate (light blue solid line), dissolved CH_4 (blue solid line), and CH_4 solubility (blue dashed line) profiles in different sediments **(B–D)** (after Flury et al., 2016).

of SMTZ and the gas front depth are closely coupled. As discussed previously, seabed erosion might cause a significant change in both the gas front depths and the SMTZ locations. Since the rapid development of dam projects and soil-water conservation projects in the Yangtze River catchment, the sediment discharge into the estuary has dramatically decreased (Guo et al., 2021; Luan et al., 2021; Yang et al., 2022a). The mean sediment discharge during the first decade after the closure of the Three Gorges Dam in 2003 dropped to a relatively low level (145 Mt yr^{-1}), which was only approximately 30% of the value in 1950–1968 (Yang et al., 2021). Shallow water areas between 5 m and 20 m in the Yangtze subaqueous delta and the northern Hangzhou Bay have experienced remarkable erosion (Xie et al., 2013; Guo et al., 2021). From 1989 to 2018, the volume of seabed erosion in the whole Jinshan Deep Trough area was nearly 162.7×10^6 m^3, and the average erosion thickness exceeded 2.4 m (Zhang et al., 2021). Some pockmarks and mounds were observed in these eroded areas, indicating that the gas migration and seepages responded quickly to the recently increasing seabed erosion (Figure 8).

The gas front depth could fluctuate over different time scales in response to the change in environmental factors, including porewater salinity, sediment temperature, and seafloor hydrostatic pressure (Wever et al., 2006; Diez et al., 2007; Martinez-Carreño and Garcia-Gil, 2013). Over a seasonal scale, Sun et al. (2018) reported that the concentration of CH_4 in bottom water in summer and autumn was significantly higher than that in spring and winter in the East China Sea. The seasonal variability of gas front depths and gas seepages was also observed in the Ría de Vigo by means of more gas plumes and shallower gas front depth in summer than in winter (Martinez-Carreño and Garcia-Gil, 2013). This could be explained by the fact that the higher sediment temperature decreases the solubility of CH_4 in interstitial water and increases gas pressure in sediments, consequently leading to more CH_4 escaping from shallow sediments during the warm season.

Moreover, global warming may trigger more CH_4 escaping from marine sediments. CH_4 is estimated to be approximately 20–40 times more effective in causing global warming than CO_2 (Letcher, 2019; IPCC, 2021). Thus, more caution should be paid to the loop of positive feedback between increasing global warming and more shallow gas seepages from the world's coastal areas.

5.3.2 Seabed instability

Marine sediments containing dissolved CH_4 can cause a reduction of soil strength, becoming fragile to trigger seabed erosion and seafloor construction subsidence (Huang and Han, 2020; Li, 2020). It is generally believed that the SMTZ depth determines the upper limit of dissolved CH_4 diffusion in shallow sediments. The gas front depth was observed to range from 2 to 5 m in

the Hangzhou Bay (Figure 7), suggesting that the dissolved CH_4 could even be found in the upper 2-m sub-bottom sediments. As discussed above, the occurrence of seabed erosion will lead to strengthening gas upward migration and shallowing the SMTZ. Continuous erosion due to sediment deficit in the study area should have induced an upward shift of the SMTZ, as indicated by the presence of dissolved CH_4 in shallower marine sediments (Wang and Liu, 2016; Song et al., 2021). Meanwhile, shallower sediments containing dissolved CH_4 will further enhance seabed erosion. Thus, positive feedback of seabed erosion induced by external factors (e.g., sediment deficit due to river damming projects) and internal factors (e.g., reduced soil strength by the presence of dissolved CH_4) could produce severe erosion, gas migration, and seepage events even under small wave conditions (Figure 12A).

The Yangtze Delta and the Hangzhou Bay are subject to storm impacts, including typhoons in summer and cold fronts in winter. Storm waves can cause sediment liquefication and submarine failures due to the sharp increase of pore pressure in water-saturated gassy sediments, leading to geological hazards or even geological disaster events (Figure 12B) (Wang and Liu, 2016; Kramer et al., 2017; Wang et al., 2019; Gupta et al., 2022). In the Hangzhou Bay, the oil and gas pipelines were reported to be destroyed a few times during typhoon events as indicated by newly produced large pockmarks (Cui et al., 2014; Li, 2020). Sometimes, the pipelines can be broken by liquefaction-induced subsidence as shown by the increased burial depth of oil pipeline reaching up to 2 m after the strike of typhoon "SWAN" in the Hangzhou Bay. More frequent and powerful storms are expected in the warming earth; thus, the instability of shallow gas-charged sediments in the highly developed coastal seas deserves more attention to build up early warming capability for hazard and disaster prediction and reduction.

6 Conclusion

Shallow gas is explored and has been found to extensively exist in the Holocene muddy sediments in the Yangtze subaqueous delta and the Hangzhou Bay as shown by the common presence of acoustic anomalous reflections including enhanced reflection, gas chimney, bright spot, acoustic blanking, and acoustic turbidity. The gas front depth does not exceed 17.5 m, and it is generally much shallower in the Hangzhou Bay than that in the Yangtze subaqueous delta because the former has, on average, smaller water depth and coarser sediments than the latter. Shallow gas is a biogenic production, and its distribution is primarily determined by the Holocene stratal thickness and water depth. Shallow gas migration is mainly controlled by overburden pressure and sediment permeability. Gas migration and seepage phenomenon (such as gas chimney, mound, pockmark, and gas plumes) are common in the study area, which are clearly enhanced by recently increasing seabed erosion because of sediment deficit. Positive feedback loops of gas migration with global warming and seabed erosion will expose coastal society to more frequent and more intense coastal geological hazards induced by shallow gas seepages. This study improves our understanding of the controlling mechanisms of dynamic changes of shallow gas in coastal seas under internal and external factors, highlighting the urgent requirement to build up early warming capability to monitor and predict shallow gas activities and associated hazards.

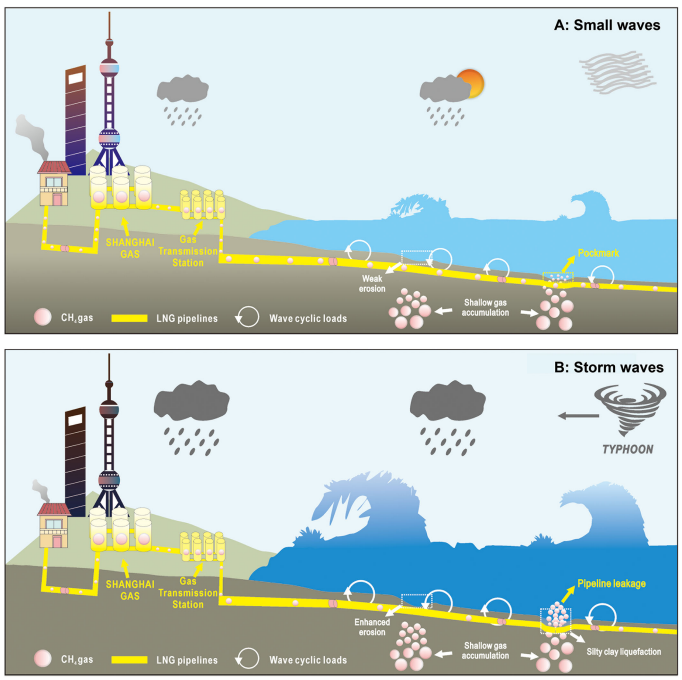

FIGURE 12
Potential geological hazards and disasters induced by the seabed instability of shallow gas-charged sediments in the highly developed coastal seas under small waves **(A)** and storm waves **(B)**.

Data availability statement

The original contributions presented in the study are included in the article/supplementary material. Further inquiries can be directed to the corresponding author.

Author contributions

LS collected and analyzed the data and wrote the manuscript. DF conceived the idea, designed the experiments, analyzed the data, and revised the manuscript. JS and XG collected and analyzed the data, and revised the manuscript. All authors contributed to the article and approved the submitted version.

Funding

This study was supported by the Innovation Program of Shanghai Municipal Education Commission (2021-01-07-00-07-E00093), the National Natural Science Foundation of China (NSFC-41976070 and 42206062), the Open Foundation of Zhoushan Field Scientific Observation and Research Station for Marine Geo-hazards, China Geological Survey (ZSORS-22-11), and the Fundamental Research Funds for the Central Universities (No. ZD-21-202101).

Conflict of interest

The authors declare that the research was conducted in the absence of any commercial or financial relationships that could be construed as a potential conflict of interest.

Publisher's note

All claims expressed in this article are solely those of the authors and do not necessarily represent those of their affiliated organizations, or those of the publisher, the editors and the reviewers. Any product that may be evaluated in this article, or claim that may be made by its manufacturer, is not guaranteed or endorsed by the publisher.

References

Beckers, J. M., Barth, A., Troupin, C., and Alvera-Azcárate., A. (2014). Some approximate and efficient methods to assess error fields in spatial gridding with DIVA (Data interpolating variational analysis). *J. Atmospheric Oceanic Technol.* 31, 515–530. doi: 10.1175/JTECH-D-13-00130.1

Chen, Y. F., Deng, B., and Zhang, J. (2020). Shallow gas in the Holocene mud wedge along the inner East China Sea shelf. *Mar. Pet. Geol.* 114, 104233. doi: 10.1016/j.marpetgeo.2020.104233

Chen, Y. F., Deng, B., Zhang, W. G., and Zhang, G. L. (2022). *Required data for paper publication* (Figureshare, v4). doi: 10.6084/m9.Figureshare.14768967.v4

Chen, S. S., Sun, Q. L., Lu, K., Hovland, M., Li, R. H., and Luo, P. (2017). Anomalous depressions in the northern yellow Sea basin: Evidences for their evolution processes. *Mar. Pet. Geol.* 84, 179–194. doi: 10.1016/j.marpetgeo.2017.03.030

Coughlan, M., Roy, S., O'Sullivan, C., Clements, A., O'Toole, R., and Plets, R. (2021). Geological settings and controls of fluid migration and associated seafloor seepage features in the north Irish Sea. *Mar. Pet. Geol.* 123, 104762. doi: 10.1016/j.marpetgeo.2020.104762

Cui, Z. K., Cai, C. L., Shi, J., and Zhang, Y. B. (2014). Geohazard factors and their impact on submarine pipeline safety in the East China Sea. *Mar. Geol. Front.* 30 (01), 48–54.

Cukur, D., Krastel, S., Tomonaga, Y., Çağatay, M. N., and Meydan, A. F. (2013). Seismic evidence of shallow gas from lake van, eastern Turkey. *Mar. Pet. Geol.* 48, 341–353. doi: 10.1016/j.marpetgeo.2013.08.017

Diez, R., García-Gil, S., Durán, R., and Vilas, F. (2007). Gas accumulations and their association with particle size distribution patterns in the ría de arousa seabed (Galicia, NW spain): An application of discriminant analysis. *Geo-Mar. Lett.* 27, 89. doi: 10.1007/s00367-007-0064-4

Etiope, G., Ciotoli, G., Schwietzke, S., and Schoell, M. (2019). Gridded maps of geological methane emissions and their isotopic signature. *Earth Syst. Sci. Data* 11 (1), 1–22. doi: 10.5194/essd-11-1-2019

Etiope, G., and Schwietzke, S. (2019). Global geological methane emissions: An update of top-down and bottom-up estimates. *Elementa-Sci. Anthrop.* 7, 47. doi: 10.1525/elementa.383

Fan, D., Li, C., Wang, D., Wang, P., Archer, A. W., and Greb, S. (2004). Morphology and sedimentation on open-coast intertidal flats of the changjiang delta, China. *J. Coast. Res.* 43, 23–35.

Fan, D., Wu, Y., Zhang, Y., Burr, G., Huo, M., and Li, J. (2017). South flank of the Yangtze delta: Past, present, and future. *Mar. Geol.* 392, 78–93. doi: 10.1016/j.margeo.2017.08.015

Fannin, N. (1980). The use of regional geological surveys in the North Sea and adjacent areas in the recognition of offshore hazards. *Safety in Offshore Drilling: The Role of Gas Surveys*, Kluwer Academic Publishers, Dordrecht.

Feng, X. (2017). Geochemical characterization of shallow Holocene biogenic gas source rocks in the coastal plain of Jiangsu and Zhejiang. *Nanjing University (in Chinese with English abstract).*

Fleischer, P., Orsi, T. H., Richardson, M. D., and Anderson, A. L. (2001). Distribution of free gas in marine sediments: A global overview. *Geo-Mar. Lett.* 21, 103–122. doi: 10.1007/s003670100072

Floodgate, G. D., and Judd, A. G. (1992). The origins of shallow gas. *Cont. Shelf Res.* 12 (10), 1145–1156. doi: 10.1016/0278-4343(92)90075-U

Flury, S., Røy, H., Dale, A. W., Fossing, H., Tóth, Z., Spiess, V., et al. (2016). Controls on subsurface methane fluxes and shallow gas formation in Baltic Sea sediment (Aarhus bay, Denmark). *Geochim. Cosmochim. Acta* 188, 297–309. doi: 10.1016/j.gca.2016.05.037

García-García, A., Orange, D. L., Miserocchi, S., Correggiari, A., Langone, L., Lorenson, T. D., et al. (2007). What controls the distribution of shallow gas in the Western Adriatic Sea? *Cont. Shelf Res.* 27 (3-4), 359–374. doi: 10.1016/j.csr.2006.11.003

Guo, X. J., Yan, X. X., Zheng, S. W., Wang, H. M., and Yin, P. (2021). Characteristics of high-resolution subaqueous micro-topography in the jinshan deep trough and its implications for riverbed deformation, hangzhou bay, China. *Estuar. Coast. Shelf Sci.* 250, 107147. doi: 10.1016/j.ecss.2020.107147

Gupta, S., Schmidt, C., Böttner, C., Rüpke, L., and Hartz, E. H. (2022). Spontaneously exsolved free gas during major storms as an ephemeral gas source for pockmark formation. *Geochem. Geophys. Geosyst.* 23, e2021GC010289. doi: 10.1029/2021GC010289

Hovland, M., and Judd, A. G. (1988). Seabed pockmarks and seepages: Impact on geology, biology and the marine environment. *Graham Trotman*. 244, 590–591. doi: 10.13140/RG.2.1.1414.1286

Hu, X. Q., Gu, Z. F., Zhang, X. H., Zhao, L. H., and Xing, Z. H. (2016). Seismic shape features and distribution of shallow gas in the sea area off the Yangtze river estuary. *Mar. Geol. Quat. Geol.* 36 (01), 151–157.

Hu, Y., Li, H. D., and Xu, J. (2012). Shallow gas accumulation in a small estuary and its implications: A case history from in and around xiamen bay. *Geophys. Res. Lett.* 39, L24605. doi: 10.1029/2012GL054478

Huang, Y., and Han, X. (2020). Features of earthquake-induced seabed liquefaction and mitigation strategies of novel marine structures. *J. Mar. Sci. Eng.* 8 (5), 310. doi: 10.3390/jmse8050310

Hustoft, S., Bünz, S., and Mienert, J. (2010). Three-dimensional seismic analysis of the morphology and spatial distribution of chimneys beneath the nyegga pockmark field, offshore mid-Norway. *Basin Res.* 22, 465–480. doi: 10.1111/j.1365-2117.2010.00486.x

IPCC (2021). *Climate change 2021: The physical science basis: Contribution of working group I to the sixth assessment report of the intergovernmental panel on climate change* (Cambridge: Cambridge University Press).

Jaśniewicz, D., Klusek, Z., Brodecka-Goluch, A., and Bolałek, J. (2019). Acoustic investigations of shallow gas in the southern Baltic Sea (Polish exclusive economic zone): a review. *Geo-Mar Lett.* 39, 1–17. doi: 10.1007/s00367-018-0555-5

Judd, A., and Hovland, M. (2007). *Seabed fluid flow: The impact on geology, biology and the marine environment* (Cambridge University Press), 475.

Koch, S., Berndt, C., Bialas, J., Haeckel, M., Crutchley, G., Papenberg, C., et al. (2015). Gas-controlled seafloor doming. *Geology* 43 (7), 571–574. doi: 10.1130/G36596.1

Kramer, K., Holler, P., and Herbst, G. (2017). Abrupt emergence of a large pockmark field in the German bight, southeastern north Sea. *Sci. Rep.* 7 (1), 5150. doi: 10.1038/s41598-017-05536-1

Letcher, T. M. (2019). Why do we have global warming? *Manage. Glob. Warm.* 1, 3–15. doi: 10.1016/B978-0-12-814104-5.00001-6

Li, X. F. (2020). Damage and repair of subsea pipelines in shallow gas areas. *Oil. Gas. Stor. Transp.* 11, 1310–1315.

Li, P., Du, J., Liu, L. J., Cao, C. X., and Xu, Y. Q. (2010). Distribution characteristics of offshore shallow gas in China. *Chin. J. Geol. Hazards. Prev.* 21 (01), 69–74.

Li, C., Fan, D., Yang, S., and Cai, J. (2008). Characterization and formation of the late quaternary incised valley sequence in the estuarine delta region of China. *J. Paleogeogr.* 10 (1), 87–97. doi: 10.2110/pec.06.85.0141

Li, G. X., Li, P., Liu, Y., Qiao, L. L., Ma, Y. Y., Xu, J. S., et al. (2014). Sedimentary system response to the global sea level change in the East China seas since the last glacial maximum. *Earth-Sci. Rev.* 139, 390–405. doi: 10.1016/j.earscirev.2014.09.007

Lin, C. M., Li, Y. L., Zhuo, H. C., Shurr, G. W., Ridgley, J. L., Zhang, Z. P., et al. (2010). Features and sealing mechanism of shallow biogenic gas in incised valley fills (the qiantang river, eastern china): A case study. *Mar. Pet. Geol.* 27 (4), 909–922. doi: 10.1016/j.marpetgeo.2009.11.006

Lin, C. M., Zhang, X., Xu, Z. Y., Deng, C. W., Yin, Y., and Cheng, Q. Q. (2015). Sedimentary characteristics and accumulation conditions of shallow-biogenic gas for the late quaternary sediments in the changjiang river delta area. *Adv. Earth Sci.* 30 (05), 589–601.

Liu, Y. F. (2019). Recent evolution process and influencing factors of jinshan deep trough in the hangzhou bay. *East China Normal Univ*.

Liu, X. Y., Feng, X. L., Sun, Y. F., Chen, Y. L., Tang, Q. H., Zhou, X. H., et al. (2019). Acoustic and biological characteristics of seafloor depressions in the north yellow Sea basin of China: Active fluid seepage in shallow water seafloor. *Mar. Geol.* 414, 34–46. doi: 10.1016/j.margeo.2019.05.002

Luan, H. L., Ding, P. X., Yang, S. L., and Wang, Z. B. (2021). Accretion-erosion conversion in the subaqueous Yangtze delta in response to fluvial sediment decline. *Geomorphology* 382, 107680. doi: 10.1016/j.geomorph.2021.107680

Martinez-Carreño, N., and Garcia-Gil, S. (2013). The Holocene gas system of the ria de vigo (NW spain): Factors controlling the location of gas accumulations, seeps and pockmarks. *Mar. Geol.* 344, 82–100. doi: 10.1016/j.margeo.2013.07.012

Mogollón, J. M., Dale, A. W., Fossing, H., and Regnier, P. (2012). Timescales for the development of methanogenesis and free gas layers in recently-deposited sediments of arkona basin (Baltic Sea). *Biogeosciences* 9, 1915–1933. doi: 10.5194/bg-9-1915-2012

Mogollón, J. M., Dale, A. W., and Tensen., J. B. (2013). A method for the calculation of anaerobic oxidation of methane rates across regional scales: An example from the belt seas and the sound (North Sea–Baltic Sea transition). *Geo-Mar. Lett.* 33, 299–310. doi: 10.1007/s00367-013-0329-z

Ni, Y. Q., Geng, Z. X., and Zhu, J. Z. (2003). Study on the hydrodynamic characteristics of hangzhou bay. *Hydrodyn. Res. Prog.* 18 (4), 439–445.

Nyman, A., Rinne, H., Salovius-Lauren, S., and Vallius, H. (2020). The distribution and characterization of gas domes in lumparn bay, Åland islands, northern Baltic Sea. *J. Mar. Syst.* 208, 103359. doi: 10.1016/j.jmarsys.2020.103359

Qu, C. W., Zhang, X., Lin, C. M., Chen, S. Y., Li, Y. L., Pan, F., et al. (2013). Characteristics of capillary sealing mechanism of late quaternary shallow biogenic gas in the hangzhou bay area. *Adv. Earth Sci.* 28 (2), 209–220.

Rasmussen, R. A., and Khalil, M. A. (1986). Atmospheric trace gases: Trends and distributions over the last decade. *Science* 232 (4758), 1623–1624. doi: 10.1126/science.232.4758.1623

Ren, F., Fan, D., Wu, Y., and Zhao, Q. (2019). The evolution of hypoxia off the changjiang estuary in the last 3000 years: Evidence from benthic foraminifera and elemental geochemistry. *Mar. Geol.* 417, 106039. doi: 10.1016/j.margeo.2019.106039

Rice, D. D., and Claypool, G. E. (1981). Generation, accumulation, and resource potential of biogenic gas. *AAPG Bulletin.* 65 (1), 5–25. doi: 10.1306/2F919765-16CE-11D7-8645000102C1865D

Schneider von Deimling, J., Weinrebe, W., Tóth, Zs., Fossing, H., Endler, R., Rehder, G., et al. (2013). A low frequency multibeam assessment: Spatial mapping of shallow gas by enhanced penetration and angular response anomaly. *Mar. Pet. Geol.* 44, 217–222. doi: 10.1016/j.marpetgeo.2013.02.013

Sills, G. C., and Wheeler, S. J. (1992). The significance of gas for offshore operations. *Cont. Shelf Res.* 12, 1239–1250. doi: 10.1016/0278-4343(92)90083-V

Song, Y. P., Sun, Y. F., Song, B. H., Dong, L. F., and Du, X. (2021). Comparative study on the liquefaction properties of seabed silt under wave loading in the huanghe river delta. *Acta Oceanol. Sin.* 43 (06), 129–138.

Southon, J., Kashgarian, M., Fontugne, M., Metivier, B., and Yim, W. W. S. (2002). Marine reservoir corrections for the Indian Ocean and southeast Asia. *Radiocarbon* 44, 167–180.

Stuiver, M., and Reimer, P. J. (1993). Extended (super 14) C data base and revised CALIB 3.0 (super 14) C age calibration program. *Radiocarbon* 35 (1), 215–230.

Su, J., Fan, D., Leng, W., Chen, L., and Yin, P. (2017). Postglacial sequence stratigraphy and sedimentary environment evolution of the Yangtze river subaqueous delta. *J. Palaeogeogr.* 19 (03), 541–556.

Su, J., Fan, D., Liu, J., and Wu, Y. (2020). Anatomy of the transgressive depositional system in a sediment-rich tide-dominated estuary: The paleo-Yangtze estuary, China. *Mar. Pet. Geol.* 121, 104588. doi: 10.1016/j.marpetgeo.2020.104588

Sumer, B. M., Truelsen, C., and Fredsøe, J. (2006). Liquefaction around pipelines under waves. *J. Waterw. Port Coast. Ocean Eng.* 132 (4), 266–275. doi: 10.1061/(ASCE)0733-950X(2006)132:4(266)

Sun, M. S., Zhang, G. L., Ma., X., Cao, X. P., Mao, X. Y., Ye, W. W., et al. (2018). Dissolved methane in the East China Sea: Distribution, seasonal variation and emission. *Mar. Chem.* 202, 12–26. doi: 10.1016/j.marchem.2018.03.001

Toker, M., and Tur, H. (2021). Shallow seismic characteristics and distribution of gas in lacustrine sediments at lake erçek, Eastern Anatolia, Turkey, from high–resolution seismic data. *Environ. Earth Sci.* 80, 727. doi: 10.1007/s12665-021-10039-4

Ulyanova, M., Sivkov, V., Kanapatskij, T., Sigalevich, P., and Pimenov, N. (2012). Methane fluxes in the southeastern Baltic Sea. *Geo-Mar Lett.* 32, 535–544. doi: 10.1007/s00367-012-0304-0

Visnovitz, F., Bodnár, T., Tóth, Z., Spiess, V., Kudó, I., Timár, G., et al. (2015). Seismic expressions of shallow gas in the lacustrine deposits of lake balaton, Hungary. *Near Surf Geophys.* 13, 433–446. doi: 10.3997/1873-0604.2015026

Wang, H., and Liu, H. J. (2016). Evaluation of storm wave-induced silty seabed instability and geo-hazards: A case study in the yellow river delta. *Appl. Ocean Res.* 58, 135–145. doi: 10.1016/j.apor.2016.03.013

Wang, H., Liu, H. J., Zhang, M. S., and Wang, X. H. (2016). Wave-induced seepage and its possible contribution to the formation of pockmarks in the huanghe (Yellow) river delta. *Chin. J. Oceanol. Limnol.* 34 (1), 200–211. doi: 10.1007/s00343-015-4245-0

Wang, Z. H., Saito, Y., Zhan, Q., Nian, X. M., Pan, D. D., Wang, L., et al. (2018). Three-dimensional evolution of the Yangtze river mouth, China during the Holocene: Impacts of sea level, climate and human activity. *Earth-Sci. Rev.* 185, 938–955. doi: 10.1016/j.earscirev.2018.08.012

Wang, H., Su, L., Zhang, M. S., and Liu, H. J. (2020). Effects of storm wave-induced liquefaction on lateral deformation of monopile-type offshore wind turbines in silt seabed. *J. Mar. Environ. Eng.* 10 (3), 225–242.

Wang, Y., Yan, X. X., Wang, Z. H., Zhao, B. C., and Zhan, Q. (2019). Shallow seismic facies characteristics of the modern underwater delta of the Yangtze river. *Mar. Geol. Quat. Geol.* 39 (02), 114–122.

Wang, M. J., Zheng, H. B., Yang, S. Y., and Fan, D. D. (2012). Environmental information in subaqueous Yangtze river delta since Holocene. *J. Tongji Univ. (Nat. Sci.)* 40 (03), 473–477.

Wever, T. F., Lühder, R., and Knispel, U. (2006). Potential environmental control of free shallow gas in the seafloor of eckernförde bay, Germany. *Mar. Geol.* 225, 1–4. doi: 10.1016/j.margeo.2005.08.005

Whiticar, M. J. (1999). Carbon and hydrogen isotope systematics of bacterial formation and oxidation of methane. *Chem. Geol.* 161, 291–314. doi: 10.1016/S0009-2541(99)00092-3

Xie, D. F., Pan, C. H., Cao, Y., and Zhang, B. H. (2013). Decadal variations in the erosion/deposition pattern of the hangzhou bay and their mechanism in recent 50a. *Acta Oceanol. Sin.* 35 (04), 121–128.

Xie, D. F., Pan, C. H., Wu, X. G., Gao, S., and Wang, Z. B. (2017). Local human activities overwhelm decreased sediment supply from the changjiang river: Continued rapid accumulation in the hangzhou bay-qiantang estuary system. *Mar. Geol.* 392, 66–77. doi: 10.1016/j.margeo.2017.08.013

Xu, Y. S., Wu, H. N., Shen, J. S., and Zhang, N. (2017). Risk and impacts on the environment of free-phase biogas in quaternary deposits along the coastal region of shanghai. *Ocean Eng.* 137, 129–137. doi: 10.1016/j.oceaneng.2017.03.051

Yang, J. H., Lai, X. H., and Chen, Z. X. (2021). Analysis of submarine pockmarked landforms and their genesis in the waters of Qingbang Island, eastern Zhoushan Islands. *J Appl. Oceanogr.* 40 (02), 251–259.

Yang, X. D., Chun, M. H., Luo, X. Q., and Yao, Z. G. (2022b). Research on application of seismic attribute analysis in identification of subsea shallow gas. *Coast. Eng.* 01), 26–36.

Yang, H. F., Li, B. C., Yang, S. L., Zhang, Z. L., Xu, K. H., Chen, C. P., et al. (2022a). Impacts of large projects on the sediment dynamics and evolution of the hengsha shoal in the Yangtze delta. *Ocean Eng.* 261, 112030. doi: 10.1016/j.oceaneng.2022.112030

Yang, S. L., Milliman, J. D., Li, P., and Xu, K. (2011). 50,000 dams later: Erosion of the Yangtze river and its delta. *Glob. Planet. Change* 75 (1-2), 14–20. doi: 10.1016/j.gloplacha.2010.09.006

Yang, X. D., Yao, Z. G., Chun, M. H., and Luo, X. Q. (2019). Research on detection technology of subsea well mouth. *Coast. Eng.* 38 (03), 232–239.

Ye, Y. C., Chen, J. R., Pan, G. F., and Liu, K. (2003). A study of formation cause, existing characteristics of the shallow gas and its danger to engineering. *Donghai Mar. Sci.* 01), 27–36.

Zhan, Q., Wang, Z., Xie, Y., Xie, J., and He, Z. (2012). Assessing C/N and $\delta^{13}C$ as indicators of Holocene sea level and freshwater discharge changes in the subaqueous Yangtze delta, China. *Holocene* 22, 697–704. doi: 10.1177/0959683611423685

Zhang, X., and Lin, C. M. (2017). Characteristics and accumulation model of the late quaternary shallow biogenic gas in the modern changjiang delta area, eastern China. *Pet. Sci.* 14, 261–275. doi: 10.1007/s12182-017-0157-2

Zhang, X., Lin, C. M., Gao, S., Robert, W. D., Qu, C. W., Yin, Y., et al. (2013a). Sedimentary sequence and distribution pattern of filling in qiantang river incised valley. *J. Paleogeogr.* 15 (06), 839–852.

Zhang, X., Lin, C. M., Li, Y. L., Qu, C. W., and Wang, S. J. (2013b). Sealing mechanism for cap beds of shallow-biogenic gas reservoirs in the qiantang river incised valley, China. *Cont. Shelf Res.* 69, 155–167. doi: 10.1016/j.csr.2013.09.006

Zhang, X. Y., Dai, Z. J., Feng, L. X., and Huang, Z. M. (2021). Study of the erosion-siltation state of the Jinshan deep trough on the north coast of Hangzhou Bay. *Adv Mar. Sci.* 39 (04), 535–547.

Zhang, G. L., Zhang, J., Kang, Y. B., and Liu, S. M. (2004). Distributions and fluxes of methane in the East China Sea and the yellow Sea in spring. *J. Geophys. Res.* 109, C07011. doi: 10.1029/2004JC002268

Zhang, G. L., Zhang, J., Liu, S. M., Ren, J. L., Xu, J., and Zhang, F. (2008). Methane in the changjiang (Yangtze river) estuary and its adjacent marine area: Riverine input, sediment release and atmospheric fluxes. *Biogeochemistry* 91 (1), 71–84. doi: 10.1007/s10533-008-9259-7